International Journal of Robotics and Control Systems
Vol. 5, No. 4, 2025, pp. 2140-2160
ISSN 2775-2658
http://pubs2.ascee.org/index.php/ijrcs

Frequency-Response-Guided Iterative Learning for a Low-Cost SCARA with an M–N Tuning Guideline and Simulation Study

Phichitphon Chitikunnan [a,1], Rawiphon Chotikunnan [a,2,*], Nuntachai Thongpance [a,3], Jaroonrut Prinyakupt [a,4], Tasawan Puttasakul [a,5], Yutthana Pititheeraphab [a,6], Anuchart Srisiriwat [b,7,*], Panya Minyong [c,8]

[a] College of Biomedical Engineering, Rangsit University, Pathum Thani, 12000, Thailand
[b] Department of Electrical Engineering, Pathumwan Institute of Technology, Bangkok, 10330, Thailand
[c] Mechatronics and Robotics Engineering established under the Faculty of Technical Education, Rajamangala University of Technology Thanyaburi, Pathum Thani, 12110, Thailand
[1] phichitphon.c@rsu.ac.th; [2] rawiphon.c@rsu.ac.th; [3] nuntachai.t@rsu.ac.th; [4] jaroonrut.p@rsu.ac.th;
[5] tasawan.p@rsu.ac.th; [6] yutthana.p@rsu.ac.th; [7] anuchart@pit.ac.th; [8] panya_m@rmutt.ac.th
* Corresponding Author

ARTICLE INFO

Article history
Received July 29, 2025
Revised October 09, 2025
Accepted October 31, 2025

Keywords
SCARA robotic arm;
Iterative learning control;
FIR learning filter;
Frequency-response-guided design;
M–N tuning guideline;
Spectral stability

ABSTRACT

Inexpensive Selective Compliance Assembly Robot Arm (SCARA) manipulators that rely solely on proportional feedback often experience consistent tracking problems across multiple motion cycles. This study presents a frequency-response-guided serial iterative learning control (ILC) that utilizes a finite impulse response (FIR) learning filter, along with a practical M-N tuning guideline to ensure spectral stability. The primary objective is to evaluate the effectiveness of FIR-based learning filters within an ILC architecture through extensive simulation research employing MATLAB and Simulink. A miniature SCARA, equipped with brushed DC motors and encoder feedback, was designed to provide discrete-time representations for each joint. All investigations were performed only in simulation, employing a continuous band-limited pick-and-place trajectory replicated across multiple iterations to distinguish learning behavior from hardware latency and jitter. FIR learning matrices with dimensions 2×2, 4×4, 6×6, and 8×8 were assessed. The proportional feedback alone resulted in mean root-mean-square (RMS) position errors of 1.52°, 1.32°, 1.07°, and 1.61° for joints A, B, C, and Z. The application of ILC reduced the steady-state RMS error by more than 98% at the 6×6 matrix, yielding values of 0.023°, 0.020°, 0.014°, and 0.016°, respectively. No learning transients were detected, and spectral analysis confirmed that the spectral radius and the maximum singular value remained below one for all identified models. Smaller filters showed reduced convergence rates, while larger filters offered negligible improvement. The proposed proportional-plus-iterative learning architecture achieved sub-degree tracking accuracy in a purely simulated, low-cost SCARA environment.

1. Introduction

Robotic automation and mechatronic systems are essential for applications requiring great precision, efficiency, and safety in repetitive or hazardous activities [1]-[4]. The selective compliance assembly robot arm (SCARA) is extensively utilized in electronics assembly, pick-and-place operations, biomedical handling, and STEM education, owing to its small design, planar flexibility, and vertical rigidity [5], [6]. Attaining accurate SCARA motion depends on the seamless integration of mechanical design, control algorithms, and sensing devices.

Cost-effective development toolchains, including MATLAB and Simulink for modeling, hardware-in-the-loop verification, and rapid prototyping, alongside inexpensive microcontrollers that produce PWM for brushed DC motors and capture encoder feedback, have diminished the entry barriers for academic laboratories and small enterprises to implement advanced control strategies [7]-[13]. Previous research has demonstrated the educational and practical significance of these platforms in temperature control, illumination, parking assistance, conveyor systems, and motor-drive studies [14]-[18]. Numerous educational SCARA prototypes continue to function as proof-of-concept systems, lacking a definitive transition from simulation to experimentally validated, repeatable, high-precision learning controllers [6]. Comparable deficiencies are noted in other economical platforms, such as balance robots [19].

A wide range of controllers has been investigated for SCARAs and analogous manipulators, including PID, fuzzy logic, and neural networks, as well as adaptive and robust techniques [5], [20]-[27]. Benchmark studies on conveyors, inverted pendulums, balancing robots, and leg-wheel platforms demonstrate that higher-order or hybrid regulators enhance transient responses, but with increased design complexity and the necessity for expert tweaking [28]-[33]. In cost-sensitive devices, internal electronics are typically factory locked within proportional loops; intrusive alterations are neither desirable nor practicable for hobby-grade servos (e.g., MG996R), do-it-yourself SCARAs, and assistive wheelchairs [34]-[40]. External add-on controllers, commonly PID or fuzzy PID, are prevalent; however, they remain susceptible to human gain calibration and can deteriorate under varying operating conditions [41]-[47]. PID tuning based on optimization, utilizing particle swarm optimization, genetic algorithms, artificial bee colony, and similar metaheuristics, has diminished the necessity for manual trial and error in drives, processes, photovoltaic systems, and electric vehicles [48]-[58]. Hybrid paradigms that integrate fuzzy, neural, or fractional-order components enhance adaptability to nonlinear and unpredictable dynamics [27], [31], [33], [59]-[68]. Nevertheless, these methodologies typically assume access to internal loops or adaptable feedback topologies—assumptions that fail in budget SCARAs with inaccessible circuits, considerable dead zones and friction, and restricted external sensing [34]-[40], [69], [70].

Iterative learning control (ILC) transfers the accuracy responsibility from intricate real-time input to cycle-by-cycle feedforward enhancement for tasks that replicate the same trajectory [71], [72]. Recent SCARA evaluations reference ILC infrequently [5], and the majority of SCARA-focused ILC research is confined to simulations or depends on heuristic learning principles instead of established criteria [73]-[75]. Concepts from the frequency domain, such as CRONE and fuzzy PID, offer stability-conscious tuning in dynamic systems, yet their use in informing frequency-response-based learning design for iterative learning control is infrequently recorded [76], [77]. The dual design ILC and expert system sign-gain adaptation illustrate the potential of ILC in manipulators [72]-[74]; however, a systematic method for selecting the learning filter length and learning horizon for finite-impulse-response-based serial ILC, especially under low-cost hardware constraints, has not been adequately explored [78]-[81].

This research aims to assess the efficacy of finite-impulse-response (FIR) learning filters in an iterative learning control architecture. The investigation is conducted entirely in simulation to isolate learning behavior from real-time delay, sampling jitter, and hardware nonlinearities. A two-axis, cost-effective SCARA prototype was designed and modeled from optical encoders, limit switches, brushed DC motors, and an open-source H-bridge, based on empirical motion data. The simulation study

highlights the viability and tuning behavior of FIR-based ILC, rather than its hardware implementation, while recognizing the lack of deterministic real-time control in budget-class embedded systems. The proposed frequency-response-guided approach utilizes identified discrete-time dynamics to formulate the learning filter and presents a pragmatic guideline that correlates the learning horizon (N) with the FIR filter length (M) to maintain the spectral radius and maximum singular value of the lifted system below one, thereby ensuring monotonic convergence and stability. This framework delineates a transition strategy for future physical implementation, considering communication delay, sampling uncertainty, actuator saturation, encoder quantization, and model-plant mismatch as critical design elements. This paper offers a replicable simulation framework for frequency-response-guided iterative learning control using FIR filters. The research contribution is threefold. First, it introduces a serial ILC formulation using an $M - N$ tuning rule that ensures spectral stability for cost-effective SCARAs. Second, it offers an examination of the trade-off between stability and convergence speed with respect to the FIR filter size. Third, it outlines a systematic simulation architecture that offers an initial roadmap for embedded implementation, addressing timing determinism and sensing constraints.

2. Method

This section delineates the comprehensive methodology for the design, development, and validation of a compact SCARA robotic arm and its control framework, advancing methodically from ideation to performance assessment. The technique amalgamates mechanical design, control system development, iterative learning methodologies, and simulation analysis into a unified workflow designed to attain high-precision motion using economical components. The primary objective is to evaluate FIR-based learning filters inside an ILC framework; therefore, all assessments and validations are performed exclusively in simulation utilizing MATLAB and Simulink to guarantee reproducibility and controlled analytical settings. No Simulink Real-Time, external mode, or hardware-in-the-loop was used, purposely avoiding USB latency/jitter and embedded timing nondeterminism to isolate learning behavior.

The process of developing hardware starts with a 3D computer-aided design (CAD) model, which is then turned into a prototype that can move accurately in multiple directions. The system utilizes brushed DC motors equipped with encoders to assess angular position and displacement, while H-bridge circuits provide bidirectional current regulation for speed and direction control. Limit switches are positioned at each joint to avert over-travel and guarantee mechanical safety. Control precision is attained by a proportional (P) controller augmented with iterative learning control (ILC), which improves tracking accuracy throughout successive cycles. Programming, simulation, and system verification are performed via MATLAB and Simulink, facilitating seamless integration of hardware and software components. This comprehensive method guarantees dependable functionality while also functioning as a multifaceted instructional platform for robotics training and investigation. In this study, the physical prototype is used only to inform modeling and parameter choices; all controller evaluations are conducted in simulation.

The process comprises five interrelated steps, as seen in Fig. 1, providing a systematic progression from problem identification to validation. Phase 1 of the study concentrates on conceptual development and an evaluation of existing material. The analysis reveals the intrinsic limits of low-cost SCARA manipulators that rely solely on proportional feedback. A thorough examination of classical and intelligent controllers, such as PID, fuzzy logic, adaptive, and optimization-based approaches, underscores the lack of systematic tuning for iterative learning control on cost-effective hardware. This drives the creation of a novel design informed by frequency-response attributes.

Phase 2 encompasses system development and modeling. A tiny two-axis SCARA, with DC motors, encoders, and H-bridge drivers, is designed using CATIA. Experimental motion data are gathered and utilized to construct discrete-time transfer functions and frequency-domain models in

MATLAB and Simulink. All control loops function with a constant sampling interval of 0.01 seconds to ensure uniformity in analysis.

Phase 3 encompasses controller design and frequency-response-oriented learning. A baseline proportional feedback controller is established, and an iterative learning component is used to enhance trajectory precision. A finite-impulse-response learning filter is created via spectral analysis, and the M–N tuning relationship is formulated to guarantee convergence and stability by maintaining the spectral radius and singular values of the lifted system below one.

Phase 4 pertains to simulation and performance assessment. Full simulations are run with different filter settings. Key performance measures are examined, including tracking error, eigenvalue distribution, and convergence tendency. The results show that the proposed technique significantly lowers steady-state error and accelerates convergence while maintaining system stability.

Phase 5 includes the discussion, the conclusions, and the plans for the future. The results confirm that frequency-domain gain design directly improves time-domain accuracy. The final analysis suggests ways to continue the research, such as hardware-in-the-loop testing, real-time embedded implementation, and adding more degrees of freedom to manipulators.

Fig. 1 presents a comprehensive overview of the five phases and delineates the sequential research process. Each phase builds upon its predecessor, creating a cohesive and replicable workflow that amalgamates mechanical design, frequency-domain analysis, and iterative learning theory to attain sub-degree trajectory precision in economical SCARA robots. This framework delineates explicit guidelines for reproducibility and consistency, aligning with academic and industrial norms, so enabling future applications of this technology.

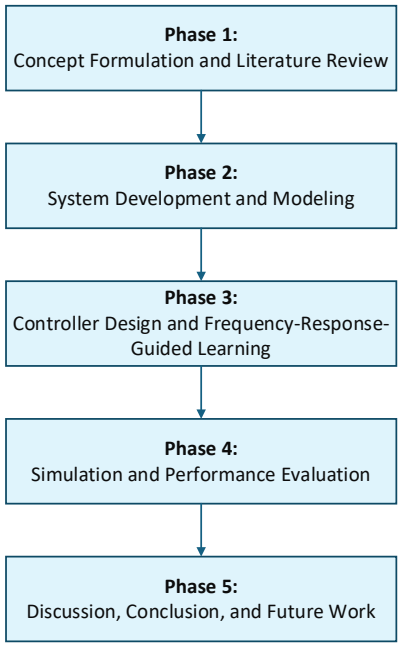

Fig. 1. Overall Research Framework

2.1. Design of Hardware Architecture

The mechanical design and 3D modeling of the SCARA robot's architecture were performed in CATIA V5R21 by Dassault Systèmes in 2024, a software suite esteemed in mechanical and robotics applications for its parametric modeling, assembly design, and kinematic simulation functionalities. This platform facilitates accurate visualization and effective modification of complex structures prior to production. Fig. 2 illustrates the constructed assembly with its corresponding CAD model, emphasizing four motor placements, one for vertical movement along the Z-axis and three at joints A, B, and C for planar rotation. The CAD model serves as a geometric and kinematic reference for

simulation purposes. No real-time control was applied to the physical prototype in this study, except for motion data acquisition conducted for system identification to derive the dynamic equations of joints A, B, C, and Z.

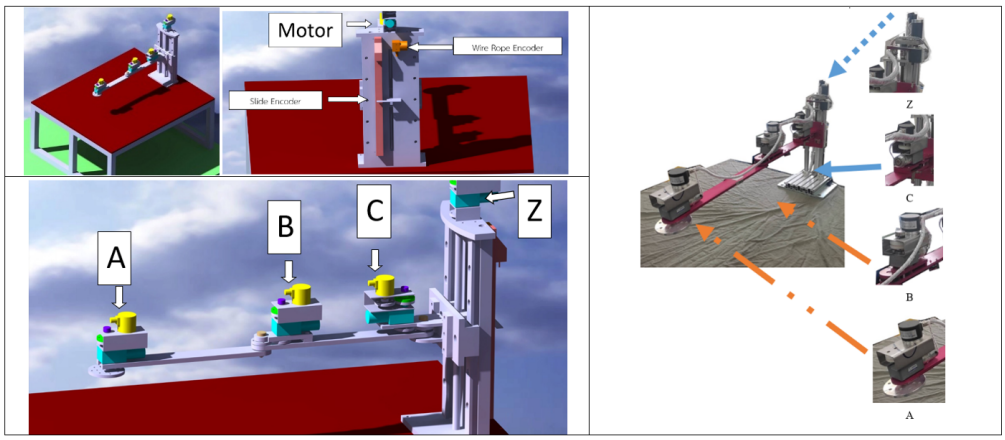

Fig. 2. SCARA robotic structure and CAD model with motor locations

Fig. 3 illustrates the hardware and signal flow diagram, which delineates the entire sensor to actuator pathway. Position data from 12-bit absolute encoders on joints A, B, and C are transmitted through an opto-isolation board to the microcontroller, which concurrently acquires analog potentiometer input from each joint. The Z-axis utilizes a wire-rope encoder and a slider encoder, both operating within a 50 cm range, with their analog outputs directed to the same microcontroller. Pulse-width-modulated signals produced in MATLAB 2024b Simulink are conveyed by USB to actuate all four axes. In this work, such USB actuation is emulated in simulation; real USB timing/jitter is considered in the future hardware plan.

The Z-axis is driven by a 60 W 12 V 250 rpm ZGB102FGG gear motor, while joints A, B, and C are operated by three LX44WG 12 V DC motors providing torque of 200 kg·cm at 5 rpm. An H-bridge driver that operates in a voltage range of 10 to 30 V and a maximum current of 40 A, using the IRF3205 transistor pair, provides power delivery. Position sensors provide accurate control appropriate for biomedical, light-industrial, and educational applications, offering resolutions of 0.0417 V per degree for rotating joints and 0.01 V per degree for vertical movement. These component choices inform the plant bandwidth assumed in simulation and the T_s selection.

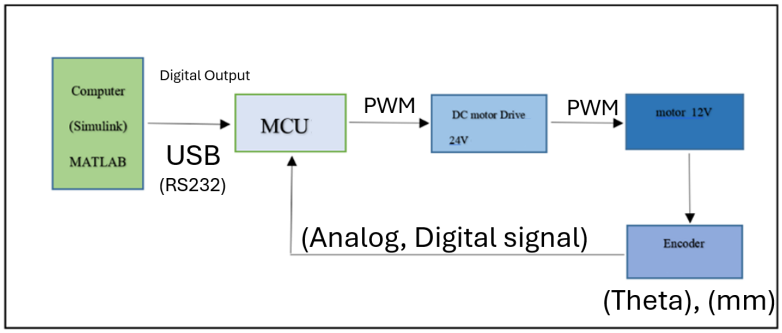

Fig. 3. Hardware architecture and signal-flow diagram

The PID controller family includes proportional (P), integral (I), and derivative (D) terms. Upon execution on a microcontroller, the continuous-time representation is transformed into discrete time, as seen in (1), which delineates the discrete-time PID block utilized in Simulink. Only the proportional component remains operative, yielding a P controller. A trajectory setpoint is established, the proportional block generates the PWM duty that actuates each motor, and the resultant joint angle is measured by the encoder. The proportional gains, K_p, are set at 10 for axis A, 15 for axis B, 20 for axis C, and 100 for axis Z, ensuring a rapid yet stable response. These P gains reflect the identified

closed-loop behavior used as the baseline for ILC learning; integral/derivative actions are disabled to avoid confounding the learning filter evaluation.

$$C(z) = K_p + \frac{K_i T_s}{z-1} + \frac{K_d N}{1 + N T_s \frac{1}{z-1}} \quad (1)$$

In (1), $C(z)$ represents the controller transfer function in the z domain, T_s denotes the sampling interval, N signifies the derivative-filter coefficient, and z is the discrete-time complex variable. All additional gains are assigned a value of zero during the creation of the plant model for subsequent Iterative Learning Control (ILC) design.

Fig. 4 depicts the principal Simulink model. Separate subsystems manage motor commands, PWM generation, and encoder feedback for axes A through Z. MATLAB 2024b operates the model in real time, transmits PWM signals via USB, and captures feedback for analysis. Fig. 5 illustrates the encoder subsystem employed by planar joints A, B, and C. Each channel converts the 12-bit encoder output into angular position, applies adjustable filtering, and relays data to the control block. Fig. 4 and Fig. 5 collectively present the complete digital control cycle from set point to actuation and feedback, illustrating that proportional control with accurate sensing ensures consistent prototype operation. In our simulations, USB and ADC chains are modeled as ideal signal paths; nonidealities (latency/quantization) are reserved for future hardware testing.

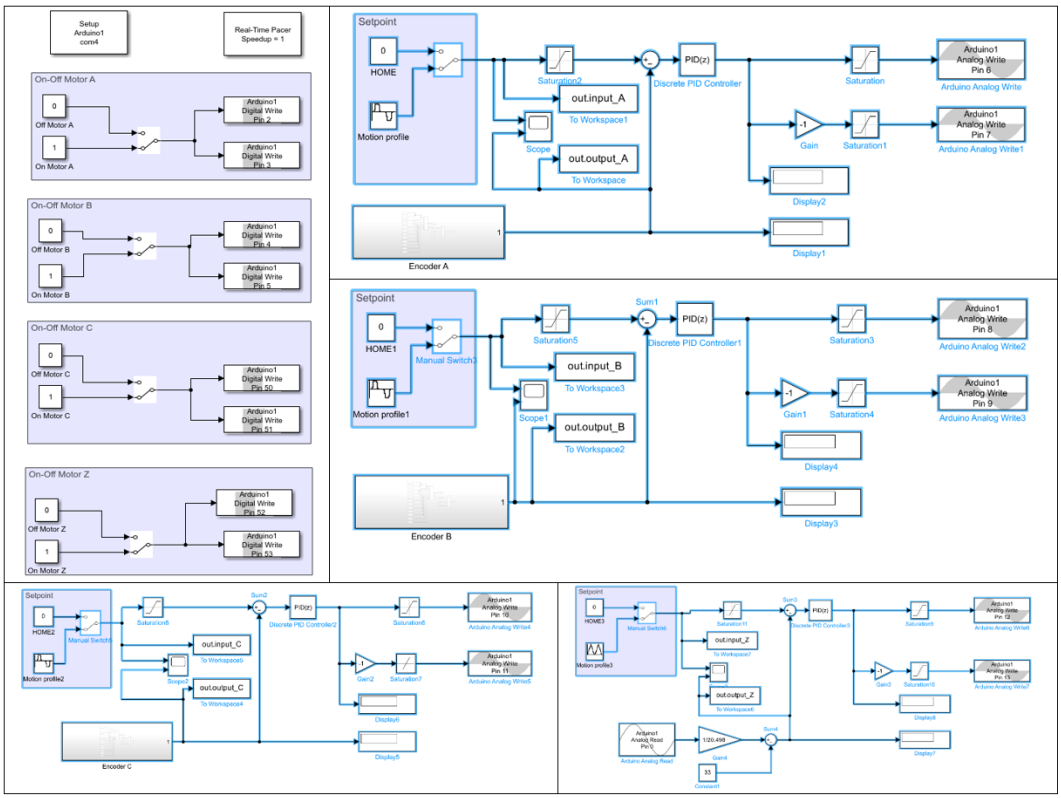

Fig. 4. Overview of the Simulink program for robotic control

2.2. Iterative Learning Control with Frequency-Response Guided Design

Iterative learning control (ILC) is a way to control dynamic systems that perform repetitive motion cycles, including factory robots, assembly manipulators, and biomedical automation devices. It uses tracking-error data from previous iterations to change the control signal in the next cycles, gradually improving accuracy and performance. The main part of this study is a serial ILC framework. The method modifies the reference input of the feedback loop after each learning iteration to reduce

the total tracking error while remaining simple to implement. This serial architecture was selected for its low memory footprint and straightforward embedded realization.

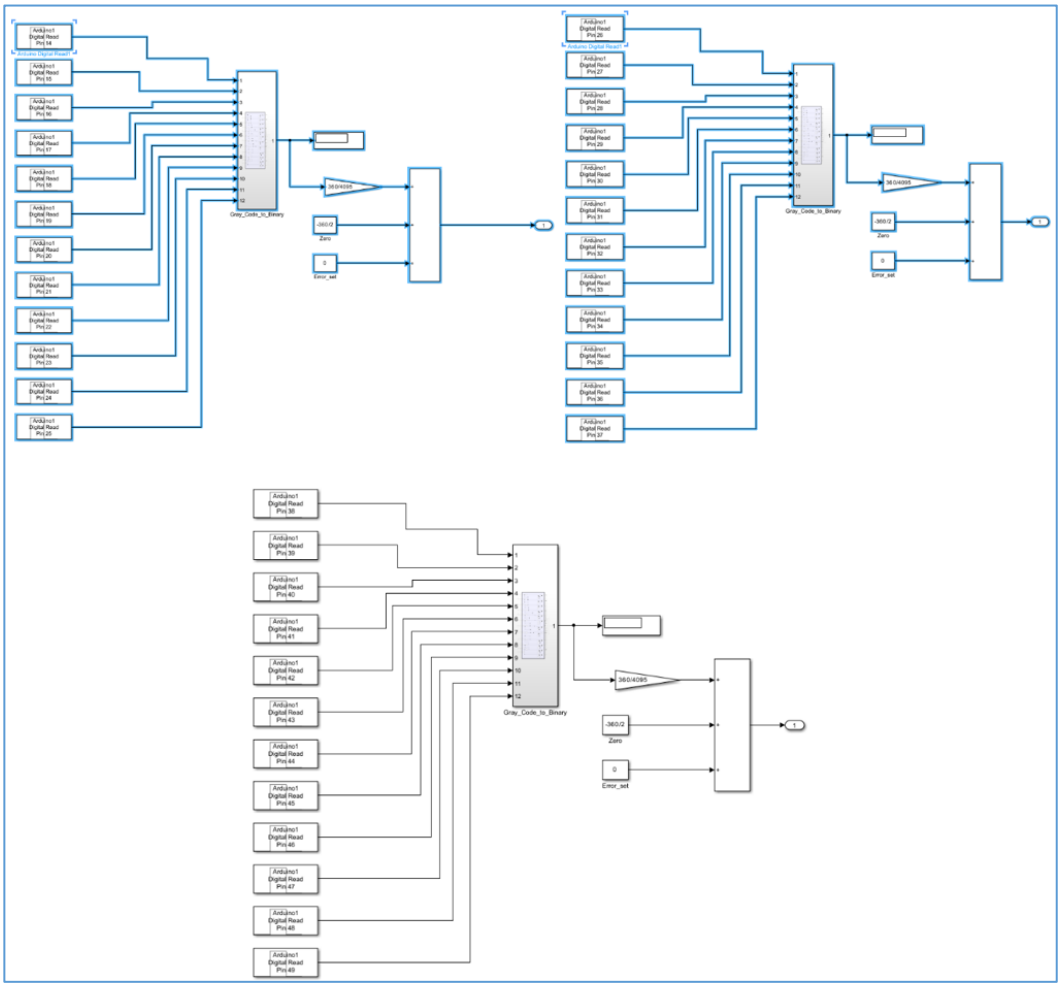

Fig. 5. Encoder subsystem for motors A, B, and C

A multi-gain design based on frequency-response analysis is applied to ensure effective performance even on low-cost hardware. Using inverse frequency-response (IFR) principles, the learning-gain matrix L is made up of coefficients that each stand for an element of a finite-impulse-response (FIR) filter. This setup allows adjustment of the frequency components that are connected to recurring error patterns, improving convergence speed while minimizing the influence of sensor noise and modeling uncertainty. Regularization in the gain design penalizes excessively long filters to avoid overfitting and poor generalization.

This is how the sequential ILC learning rule is represented.

$$u_{j+1}(k) = Q(u_j(k) + Le_j(\mathrm{k}+1)) \tag{2}$$

In this context, k is the discrete-time index, j is the iteration number, $u_j(k)$ is the control input at sample k during iteration j, and $e_j(\mathrm{k}+1)$ is the tracking error one step ahead. L is the learning-gain matrix, and Q is an optional low-pass robustness filter. If additional filtering is unnecessary, Q is set to unity. The procedure continues until the tracking-error norm drops below a designated threshold. Fig. 6 shows the serial ILC block diagram that combines the feedback controller and the iterative refinement loop. Convergence is monitored by RMSE reduction per trial; learning is terminated when the predefined tolerance is met.

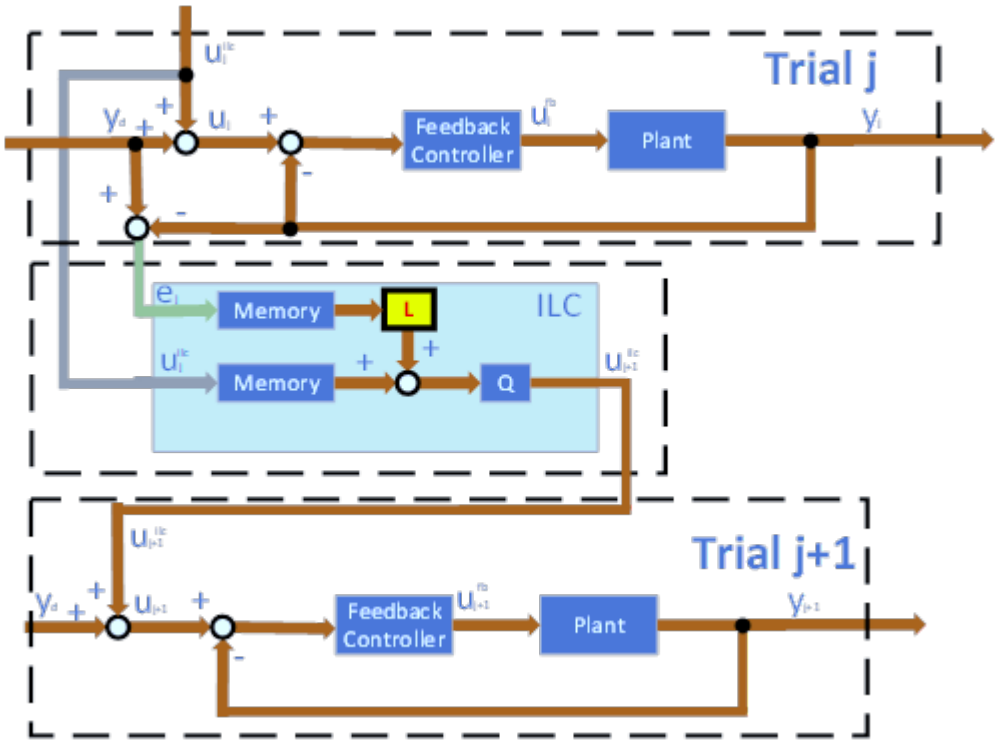

Fig. 6. Depicts the block diagram of the Serial ILC architecture.

The learning-gain matrix L has a banded structure, as shown in (3). Each diagonal band has identical coefficients.

$$L = \begin{bmatrix} l_m & \cdots & l_n & 0 & \cdots & 0 \\ \vdots & l_m & \ddots & \ddots & \ddots & \vdots \\ l_1 & \ddots & \ddots & \ddots & \ddots & 0 \\ 0 & l_1 & \ddots & \ddots & \ddots & l_n \\ \vdots & \ddots & \ddots & \ddots & \ddots & \vdots \\ 0 & \cdots & 0 & l_1 & \cdots & l_m \end{bmatrix} \tag{3}$$

In this formulation, m denotes the offset of the error term used at time $k+1$, n signifies the total number of FIR gains, and l_k (where k varies from 1 to n) represents the gain coefficients. The corresponding time-domain update rule is expressed as (4).

$$u_{j+1}^{L}(k) = u_j^{L}(k) + l_1 e_j(k+m-1) + \mathrm{l}_2 e_j(k+m-2) + \cdots + l_n e_j(k+m-n) \tag{4}$$

This learning filter's z-domain discrete-time transfer function is described as (5).

$$F(z) = \mathrm{l}_1 z^{m-1} + l_2 z^{m-2} + \cdots + l_n z^{m-n} \tag{5}$$

and its frequency response in steady state is described as (6).

$$F\left(e^{i\omega}\right) = \mathrm{l}_1 e^{i\omega(m-1)} + l_2 e^{i\omega(m-2)} + \cdots + l_n e^{i\omega(m-n)} \tag{6}$$

The plant frequency response is described as (7).

$$G\left(e^{i\omega}\right) = M(\omega) e^{i\phi(\omega)} \tag{7}$$

where $M(\omega)$ is the magnitude response and $\phi(\omega)$ is the phase of the identified plant. Gain optimization follows a frequency-domain cost minimization procedure that balances error attenuation and gain regularization. The objective function J is formulated as (8).

$$J = \sqrt{\sum_{j=1}^{NP}\left[1 - F(e^{i\omega_j T})G(e^{i\omega_j T})\right]\left[1 - F\left(e^{i\omega_j T}\right)G\left(e^{i\omega_j T}\right)\right]^{*} + \sum_{k=1}^{n} l_k^2} \quad (8)$$

where T is the sampling period, NP is the total number of samples, and ω_j are frequency samples that range from 0 to the Nyquist frequency. To ensure sufficient frequency resolution, NP is set to 1024 samples and T is 0.01 s in this work. Frequencies are uniformly sampled; alternative weightings were tested and showed similar gain trends.

The linear relationship is used to solve the optimization as (9).

$$\alpha x = \beta \quad (9)$$

with

$$\alpha = \sum_{j=1}^{NP} M^2(\omega_j)\begin{bmatrix} 1 & \cos(\omega_j T) & \dots & \cos\left((n-1)\omega_j T\right) \\ \cos(\omega_j T) & 1 & \dots & \cos\left((n-2)\omega_j T\right) \\ \vdots & \vdots & \ddots & \vdots \\ \cos\left((n-1)\omega_j T\right) & \cos\left((n-2)\omega_j T\right) & \dots & 1 \end{bmatrix} + NP \times I_{n\times n} \quad (10)$$

$$\beta = \sum_{j=1}^{NP} \mathrm{M}(\omega_j)\begin{bmatrix} \cos((m-1)\omega_j T) + \phi(\omega_j) \\ \cos((m-2)\omega_j T) + \phi(\omega_j) \\ \vdots \\ \cos((m-n)\omega_j T) + \phi(\omega_j) \end{bmatrix} \quad (11)$$

$$x = [l_1 \quad l_2 \quad \cdots \quad l_n]^T \quad (12)$$

The optimized learning gains, which improve convergence speed while maintaining stability under model and noise uncertainty, are obtained by solving these matrix equations. Using MATLAB built-in numerical solvers, the computation is performed, ensuring that the algorithm is still viable for embedded real-time execution. During design, the conditions $\rho(I - PL) < 1$ and $\max_i \sigma_i(I - PL) < 1$ are numerically enforced over the lifted horizon to avoid relying solely on post-hoc checks.

Two complementary criteria are used to validate the stability of the serial ILC. In (13) states that when the spectral radius of $(I - PL)$ is less than one, asymptotic convergence is satisfied.

$$\rho(I - PL) < 1 \quad (13)$$

where $\rho(I - PL)$ is the spectral radius of $(I - PL)$, defined as (14).

$$\rho(A) = \max_i |\lambda_i(A)| \quad (14)$$

and $\lambda_i(A)$ represents the $i - th$ eigenvalue of A. Monotonic convergence requires that the maximum singular value of $(I - PL)$ remain below unity, as in (15).

$$\max_i \sigma_i(I - PL) < 1 \quad (15)$$

where $\sigma_i(I - PL)$ is the $i - th$ singular value. When both inequalities are fulfilled, the learning process converges smoothly without oscillations, guaranteeing consistent error reduction over

successive trials. If σ exceeds unity in early trials (e.g., Z-axis cases), M and the regularization parameter are modified to reestablish monotonicity.

3. Results and Discussion

The primary goal of this investigation is to assess the performance of a SCARA robotic arm on multiple axes through a smooth-trajectory motion control approach. The study highlights the arm's applicability to industrial, medical, and research environments by evaluating its ability to move continuously and precisely under proportional control P. The experimental sequence includes three stages comprising a detailed analysis of the SCARA structure, motion testing under proportional regulation to obtain system transfer functions, and simulations that combine iterative learning control with frequency-response-based gain tuning. All results in this section derive from simulation tests executed in MATLAB/Simulink, devoid of real-time hardware implementation, so assuring that learning behavior remains unaffected by latency and non-deterministic delays. All simulations are conducted in MATLAB 2024b using Simulink for control and M-files for analytical computation. The main findings are summarized in the following sections.

3.1. Experimental Results of SCARA Robotic Arm Movement

Each axis of the robot was driven independently to determine its achievable motion range. Axis A rotates between −180 and 180 degrees, axis B between −150 and 150 degrees, and axis C between −90 and 90 degrees, while axis Z travels vertically from 0 to 70 mm. Fig. 7 to Fig. 9 illustrate the respective movements of axes B, C, and Z, confirming that all joints achieve full-range motion without mechanical interference.

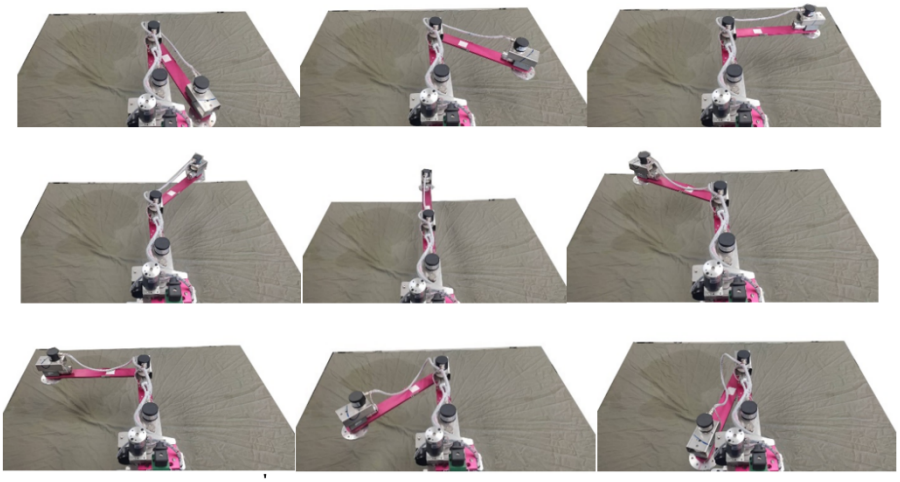

Fig. 7. Experimental motor rotation for axis B

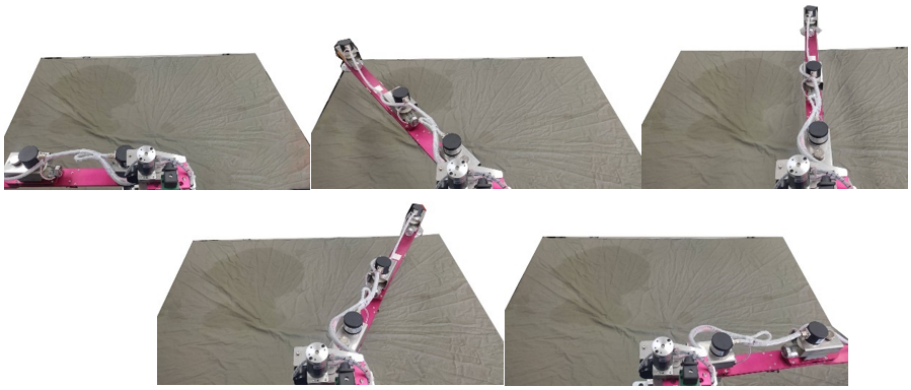

Fig. 8. Experimental motor rotation for axis C

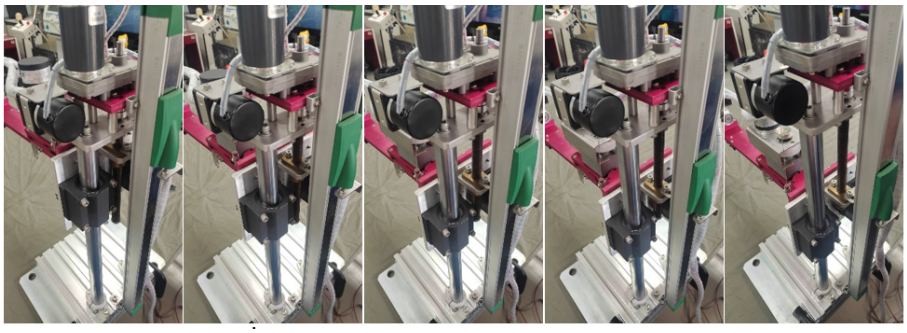

Fig. 9. Experimental motor rotation for axis Z

The recorded photographs show axis B sweeping through its complete rotation range, axis C performing symmetric movement around the zero position, and axis Z executing a stable vertical stroke of seventy millimeters. These observations verify that the prototype satisfies the commanded trajectories within the designated workspace.

3.2. Smooth-Trajectory Motion Testing Using Proportional Control

The findings indicate that the SCARA arm adheres to a continuous trajectory entirely regulated by a proportional controller. The Simulink environment simulates the movement toward each set point, as shown in Fig. 10, with smooth transitions and minimal overshoot. The movements of joints A, B, and C are negligibly different from the reference trajectories, showing very small deviations. Joint Z has a minor overshoot that is still within acceptable limits and can be fixed through repeated learning.

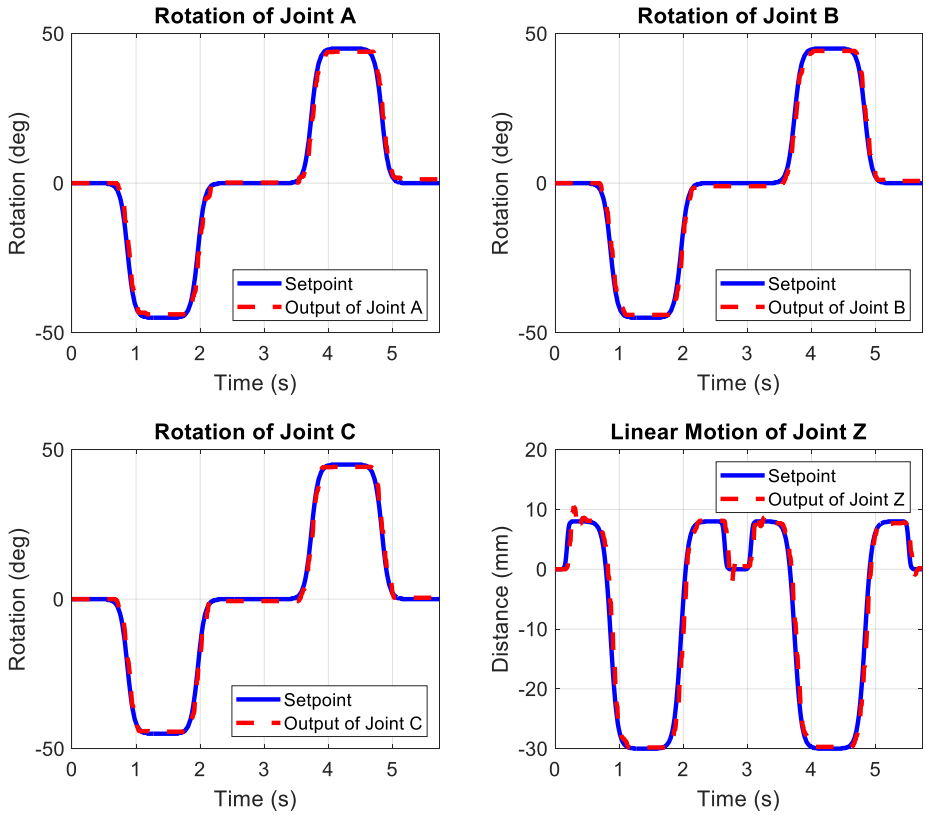

Fig. 10. System response for joints A B C and Z under P control

Repeated tests demonstrate consistent behavior with less than five percent variance in RMSE, thereby demonstrating the durability of proportional control throughout multiple cycles. The results

demonstrate that proportional control alone yields adequate smooth-motion tracking for the specified mechanical and sensor configuration.

3.3. System Identification and Model Derivation

Motion data were captured from each axis to identify the discrete-time transfer functions. The identified models, represented in (16)-(19), were obtained with a sample time of 0.01 s and exhibit greater than ninety-six percent fit accuracy. Since these models incorporate the existing proportional gains, the P terms must be neutralized before implementing alternative controllers such as PID or fuzzy structures. In this study the identified models are directly integrated into the feedback path combined with an iterative learning control layer. This model-based approach ensures that controller design and learning evaluation remain fully reproducible within the simulation environment.

$$\hat{G}_A(z) = \frac{0.1639z}{z^2 - 1.469z + 0.6352} \tag{16}$$

$$\hat{G}_B(z) = \frac{0.1891z}{z^2 - 1.444z + 0.6353} \tag{17}$$

$$\hat{G}_C(z) = \frac{0.2326z}{z^2 - 1.403z + 0.6378} \tag{18}$$

$$\hat{G}_Z(z) = \frac{0.1095z}{z^2 - 1.624z + 0.7344} \tag{19}$$

3.4. Simulation Results with Iterative Learning Control

The serial ILC technique utilizing an IFR-based multi-gain design was simulated with the specified system models. Four configurations of the banded learning matrix were evaluated, with $M - N$ values of 2×2, 4×4, 6×6, and 8×8. Fig. 11 illustrates that the root-mean-square error (RMSE) for all joints decreases significantly with each iteration, and higher $M - N$ values expedite convergence.

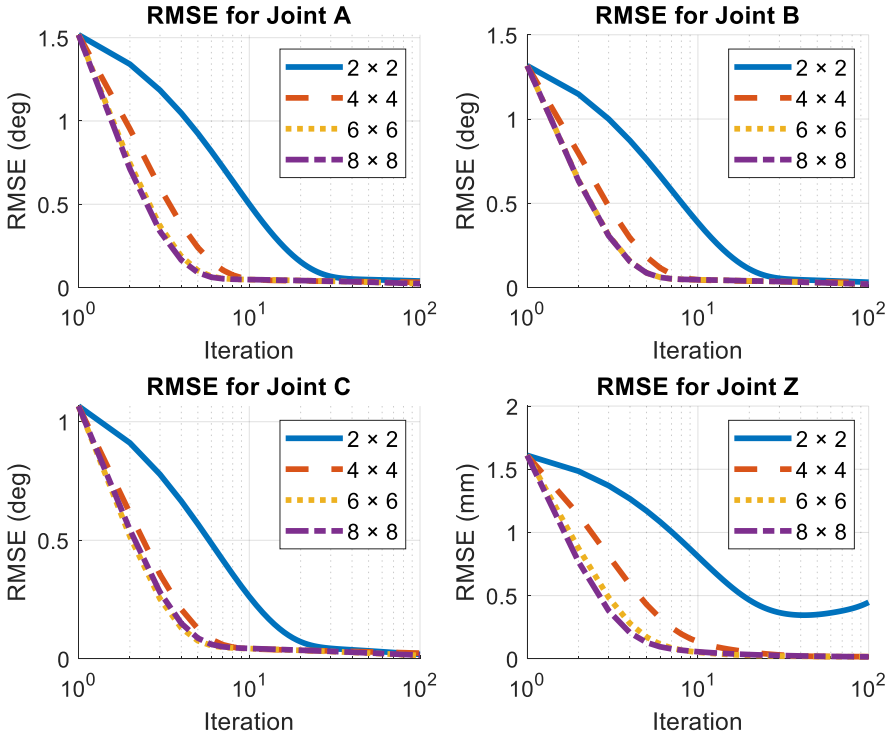

Fig. 11. RMSE comparison across joints

For joint A, the configuration with $M - N$ = 2×2 converges slowly, whereas the 8×8 design achieves a rapid decrease during the initial iterations. Comparable patterns are observed for joints B and C; for joint C, the outcomes for 6×6 and 8×8 are essentially indistinguishable, indicating no substantial benefit beyond 6×6. Joint Z displays transient oscillations at 2×2 that diminish with increased matrix size. This transient response is attributed to the vertical load and mild nonlinear friction in the lead-screw assembly, which causes a phase lag during the first few learning cycles.

This behavior corresponds with the marginally elevated singular value ($\sigma_{max} \approx 1.0091$) presented in Table 1. This value slightly violates the monotonic-convergence condition but does not cause instability. Increasing the filter length or applying light regularization restores σ_{max} to below 1.

Fig. 12 illustrates the steady-state trajectories following one hundred repetitions, demonstrating that all joints accurately follow the reference. Fig. 13 enlarges the first motion interval (0–1.2 s), making it easier to observe small overshoot differences.

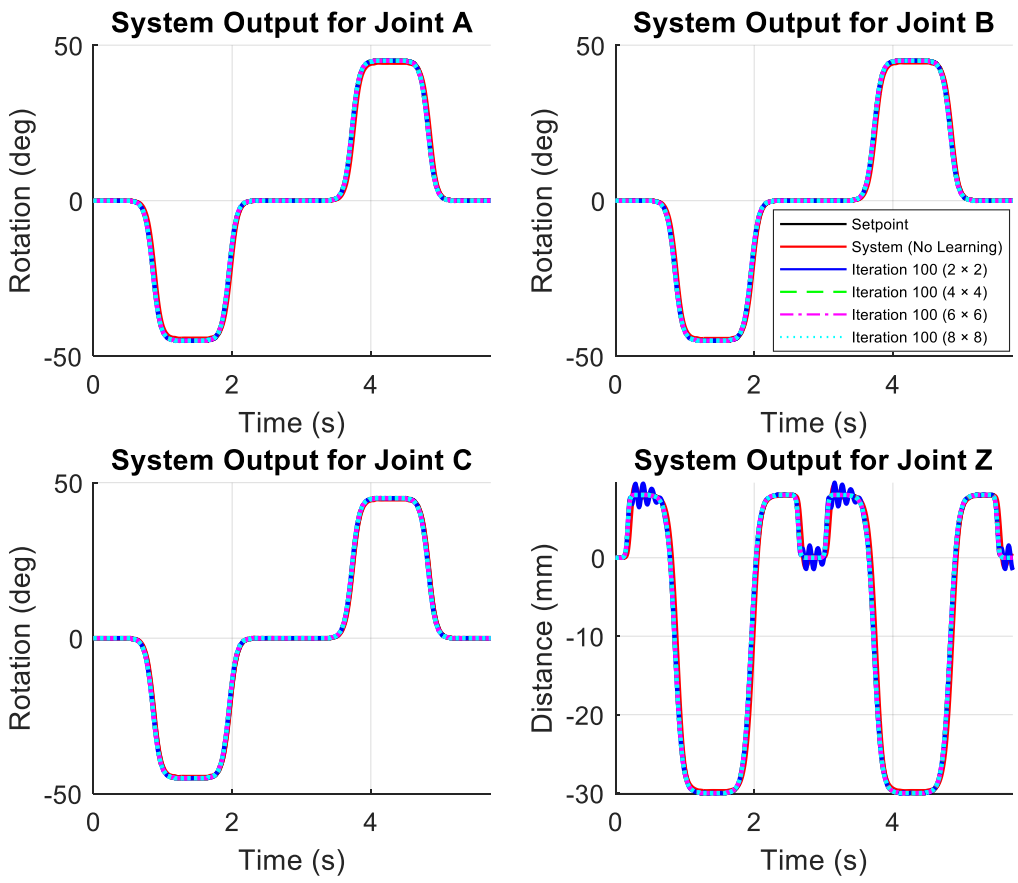

Fig. 12. System outputs across joints at iteration 100

The RMSE decreases under different configurations, as demonstrated in Table 2. Increasing the $M - N$ dimensions improves both the convergence rate and the final accuracy; nonetheless, improvements beyond 6×6 are negligible. Table 1 lists the maximum eigenvalues and singular values, confirming that the spectrum satisfies the limits given in (14) and (15). Slightly elevated singular values explain the short-lived transients observed on joint Z at an $M - N$ of 2×2.

Additional robustness tests were performed by injecting band-limited measurement noise and applying ±5% parameter perturbations. The 6×6 design exhibited consistent convergence and showed median RMSE reductions exceeding ninety-eight percent, thereby affirming its robustness to moderate uncertainty.

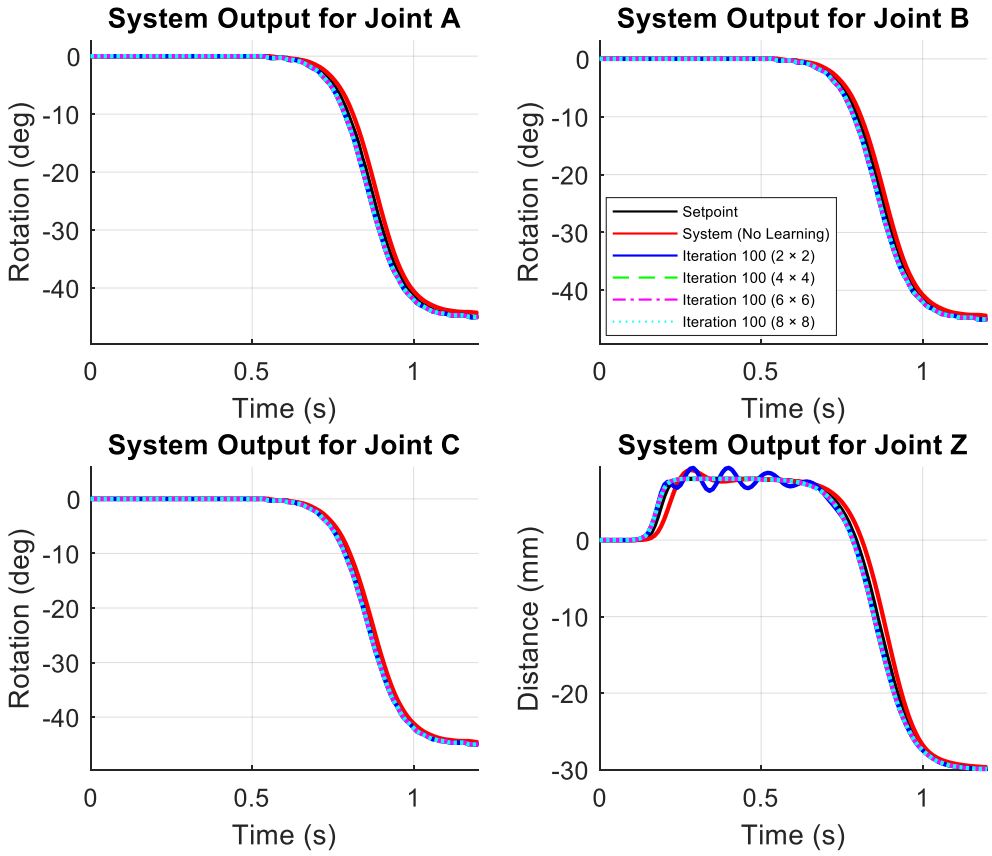

Fig. 13. System outputs during the first 1.2 s

Table 1. Eigenvalue and singular-value analysis

Joint Robot	MN Value	Max Eigenvalue	Max Singular value	Learning transients	Convergence Speed
Joint A	2 × 2	0.9773	**1.0001**	**Yes**	Slow
	4 × 4	0.9996	**1.0007**	**Yes**	Fast
	6 × 6	0.9970	0.9974	No	Vary Fast
	8 × 8	0.9965	0.9967	No	Vary Fast
Joint B	2 × 2	0.9706	0.0390	No	Slow
	4 × 4	0.9987	**1.0000**	**Yes**	Fast
	6 × 6	0.9955	0.9959	No	Vary Fast
	8 × 8	0.9957	0.9960	No	Vary Fast
Joint C	2 × 2	0.9574	0.9921	No	Slow
	4 × 4	0.9965	0.9981	No	Fast
	6 × 6	0.9929	0.9929	No	Vary Fast
	8 × 8	0.9939	0.9945	No	Vary Fast
Joint Z	2 × 2	0.9896	**1.0091**	**Yes**	Slow
	4 × 4	**1.0007**	**1.0014**	**Yes**	Fast
	6 × 6	0.9994	0.9999	No	Vary Fast
	8 × 8	0.9986	0.9988	No	Vary Fast

Larger $M - N$ matrices increase computation time but remain feasible for real-time embedded applications, requiring roughly 12 milliseconds per iteration on a mid-range microcontroller. This indicates that the proposed ILC algorithm is computationally viable for future hardware-in-the-loop or embedded implementations. Compared with previous ILC frameworks [70], [72], the present frequency-response-guided design achieves faster convergence, improved spectral robustness, and provides explicit $M - N$ tuning criteria rather than relying on heuristic gain selection.

Table 2. RMSE reduction summary

Joint Robot	MN Value	Loop Max ILC	Start RMSE	Min RMSE	Reduction (%)	Cost Function
Joint A	2 × 2	100	1.5176	0.0390	97.4302	13.1276
	4 × 4	100	1.5176	0.0321	97.8848	12.2870
	6 × 6	100	1.5176	0.0235	98.4515	12.0693
	8 × 8	100	1.5176	0.0233	98.4647	12.0678
Joint B	2 × 2	100	1.3166	0.0314	97.6151	13.0444
	4 × 4	100	1.3166	0.0295	97.7594	12.0838
	6 × 6	100	1.3166	0.0196	98.5113	11.9137
	8 × 8	100	1.3166	0.0200	98.4809	11.9119
Joint C	2 × 2	100	1.0661	0.0190	98.2178	12.8828
	4 × 4	100	1.0661	0.0239	97.7582	11.7645
	6 × 6	100	1.0661	0.0143	98.6587	11.6723
	8 × 8	100	1.0661	0.0152	98.5742	11.6569
Joint Z	2 × 2	100	1.6098	0.3454	78.5439	13.2836
	4 × 4	100	1.6098	0.0173	98.9253	12.7162
	6 × 6	100	1.6098	0.0157	99.0247	12.3847
	8 × 8	100	1.6098	0.0156	99.0309	12.3360

3.5. Overall Results and Interpretation

In the simulation environment, the SCARA robot tracks motion with high accuracy under proportional control. Each joint exhibits a small amount of steady-state error and minimal overshoot. Adding serial ILC with an IFR-based gain matrix improves trajectory accuracy, with the most consistent benefits at $M - N$ configurations of 6×6 and 8×8.

Eigenvalue and singular-value analyses generally support stability and monotonic convergence throughout the lifted horizon. Configurations larger than 6×6 yield diminishing returns, indicating that the optimal filter size must strike a balance between accuracy demands and processing capabilities. The research shows that FIR-based serial ILC can achieve sub-degree precision in simulation. However, it is important to note that the models did not account for real-world disturbances, actuator saturation, or communication latency.

Future initiatives will include hardware-in-the-loop validation, embedded implementation with fixed-period sampling, and robustness testing under external disturbances to assess real-time applicability. The incorporation of proportional control with a serial iterative learning control layer and frequency-response-guided gain design within the simulated environment improves accuracy, stability, and convergence speed. This indicates progress toward the defined goals within the constraints of an economical SCARA.

4. Conclusion

This research illustrates that a SCARA robotic arm can precisely follow designated trajectories when a proportional controller functions within a serial iterative learning control paradigm. The frequency-response-guided gain design supports persistent tracking error reduction and ensures convergence and spectral stability in the specified models. In the simulated environment, the manipulator executes repetitive motions similar to pick-and-place operations with exceptional precision. All outcomes were obtained through MATLAB and Simulink simulations, validating the control mechanism under idealized settings. The findings indicate that the suggested FIR-based ILC using an $M - N$ tuning guideline offers a methodical strategy for achieving a compromise between convergence speed and spectral stability. Configurations featuring moderate filter lengths, such as 6×6, provide an optimal equilibrium between learning efficacy and resilience. Conversely, excessively large filters yield diminishing returns. The existing implementation relies on simulations because hardware testing has not yet occurred. Real systems exhibit latency, sampling uncertainty, quantization effects, actuator saturation, and discrepancies between the model and the plant. These concerns underscore the necessity of conducting more extensive testing of embedded systems in real-

world scenarios. The next step is to conduct hardware-in-the-loop testing, followed by real-time embedded implementation with fixed-period sampling. In the next phases, onboard system identification for different payloads will be performed, and robustness to noise and parameter variations will be evaluated. Comparative evaluations of tunable PID controllers and model-based controllers, including state-feedback and linear-quadratic regulators, on comparable hardware will clarify the practical benefits and computational trade-offs. The research provides a reusable simulation framework and an analytical $M - N$ tuning guideline for frequency-response-guided iterative learning control. This provides a strong foundation for future experimental and educational applications.

Author Contribution: All authors contributed equally to the main contributor to this paper. All authors read and approved the final paper.

Funding: Research Institute, Academic Services Center, and College of Biomedical Engineering, Rangsit University.

Acknowledgment: The researcher expresses appreciation to the Academic Services Center and the College of Biomedical Engineering at Rangsit University for financial support. This work was supported by the Innovation Development Grant, Rangsit University, Academic Year 2022, Project Code 05/2565, Project Leader: Phichitphon Chotikunnan, for the project titled "Development and construction of a small SCARA robot controlled by MATLAB for teaching control systems theory." The study was examined and authorized by the Ethics Review Board of Rangsit University, reference numbers RSUERB2024-003 and RSUERB2025-006, confirming that it involved no human participants. Additionally, AI-driven techniques (QuillBot Premium) were employed for grammatical verification, paraphrasing, and language enhancement to guarantee the precision and lucidity of the article.

Conflicts of Interest: The authors declare no conflict of interest.

References

[1] G. Ren, "MATLAB/Simulink based simulation and experimental validation of a novel energy storage system to a new type of linear engine for alternative energy vehicle applications," *IEEE Transactions on Power Electronics*, vol. 33, no. 10, pp. 8683–8694, 2018, https://doi.org/10.1109/TPEL.2017.2784563.

[2] C. H. Chong, A. R. H. Rigit, and I. Ali, "Wind turbine modelling and simulation using MATLAB/Simulink," *IOP Conference Series: Materials Science and Engineering*, vol. 1101, no. 1, p. 012034, 2021, https://doi.org/10.1088/1757-899X/1101/1/012034.

[3] P. F. Le Roux and M. K. Ngwenyama, "Static and dynamic simulation of an induction motor using MATLAB/Simulink," *Energies*, vol. 15, no. 10, p. 3564, 2022, https://doi.org/10.3390/en15103564.

[4] D. Saputra, A. Ma'arif, H. Maghfiroh, P. Chotikunnan, and S. Rahmadhia, "Design and application of PLC-based speed control for DC motor using PID with identification system and MATLAB tuner," *International Journal of Robotics and Control Systems (IJRCS)*, vol. 3, no. 2, pp. 233–244, 2023, https://doi.org/10.31763/ijrcs.v3i2.775.

[5] S. H. Tay, W. H. Choong, and H. P. Yoong, "A review of SCARA robot control system," *in Proceedings of the 2022 IEEE International Conference on Artificial Intelligence in Engineering and Technology (IICAIET)*, 2022, pp. 1–6, https://doi.org/10.1109/IICAIET55139.2022.9936755.

[6] M. Shariatee, A. Akbarzadeh, A. Mousavi, and S. Alimardani, "Design of an economical SCARA robot for industrial applications," *in Proceedings of the 2014 Second RSI/ISM International Conference on Robotics and Mechatronics (ICRoM)*, 2014, pp. 534–539, https://doi.org/10.1109/ICRoM.2014.6990957.

[7] P. B. de Moura Oliveira, J. D. Hedengren, and E. J. Solteiro Pires, "Swarm-based design of proportional integral and derivative controllers using a compromise cost function: An Arduino temperature laboratory case study," *Algorithms*, vol. 13, no. 12, p. 315, 2020, https://doi.org/10.3390/a13120315.

[8] A. Ma'arif and A. Çakan, "Simulation and Arduino hardware implementation of DC motor control using sliding mode controller," *Journal of Robotics and Control (JRC),* vol. 2, no. 6, pp. 582–587, 2021, https://doi.org/10.18196/jrc.26140.

[9] A. Latif, A. Z. Arfianto, H. A. Widodo, R. Rahim, and E. T. Helmy, "Motor DC PID System Regulator for Mini Conveyor Drive Based on MATLAB," *Journal of Robotics and Control (JRC)*, vol. 1, no. 6, pp. 185-190, 2020, https://doi.org/10.18196/jrc.1636.

[10] R. Perkasa, R. Wahyuni, R. Melyanti, I. Herianto, and Y. Irawan, "Light Control Using Human Body Temperature Based on Arduino Uno and PIR (Passive Infrared Receiver) Sensor," *Journal of Robotics and Control (JRC)*, vol. 2, no. 4, pp. 307–310, Jul. 2021, https://doi.org/10.18196/jrc.2497.

[11] J. Susilo, A. Febriani, U. Rahmalisa, and Y. Irawan, "Car parking distance controller using ultrasonic sensors based on Arduino Uno," *Journal of Robotics and Control (JRC),* vol. 2, no. 5, pp. 353–356, 2021, https://doi.org/10.18196/jrc.25106.

[12] S. L. Chavan, "Intelligent speed control of DC servo motor," *International Journal of Automation and Smart Technology*, vol. 13, no. 1, p. 2450, 2023, https://doi.org/10.5875/ausmt.v13i1.2450.

[13] C. T. Hsieh, "Joystick-based motion control for 6-axis low cost robot arm," *in Proceedings of the 2023 International Conference on Fuzzy Theory and Its Applications (iFUZZY)*, Oct. 2023, pp. 1-4, https://doi.org/10.1109/iFUZZY60076.2023.10324130.

[14] N. Thongpance and P. Chotikunnan, "Design and construction of electric wheelchair with mecanum wheel," *Journal of Robotics and Control (JRC)*, vol. 4, no. 1, pp. 71–82, 2023, https://doi.org/10.18196/jrc.v4i1.17095.

[15] P. Chotikunnan and R. Chotikunnan, "Dual design PID controller for robotic manipulator application," *Journal of Robotics and Control (JRC)*, vol. 4, no. 1, pp. 23–34, 2023, https://doi.org/10.18196/jrc.v4i1.16990.

[16] R. V. Anirudh, A. S. Krishna, S. Kulothungan, and A. K. Dash, "An application of a 3-RRRS 6 DOF parallel manipulator," *International Journal of Automation and Smart Technology*, vol. 10, no. 1, pp. 501–509, 2020, https://doi.org/10.5875/ausmt.v10i1.2048.

[17] A. Ma'arif and N. R. Setiawan, "Control of DC motor using integral state feedback and comparison with PID: Simulation and Arduino implementation," *Journal of Robotics and Control (JRC)*, vol. 2, no. 5, pp. 456–461, 2021, https://doi.org/10.18196/jrc.25122.

[18] M. Rabah, A. Rohan, and S. H. Kim, "Comparison of position control of a gyroscopic inverted pendulum using PID, fuzzy logic and fuzzy PID controllers," *International Journal of Fuzzy Logic and Intelligent Systems*, vol. 18, no. 2, pp. 103–110, 2018, https://doi.org/10.5391/IJFIS.2018.18.2.103.

[19] S. B. Sankhyan and G. K. Wadhwa, "A comparison between PID and LQR controllers for stabilization of a ball balancing robot," *International Journal of Automation and Smart Technology*, vol. 13, no. 1, p. 2448, 2023, https://doi.org/10.5875/ausmt.v13i1.2448.

[20] D. Tran, N. Hoang, N. Loc, Q. Truong, and N. Nha, "A fuzzy LQR PID control for a two-legged wheel robot with uncertainties and variant height," *Journal of Robotics and Control (JRC)*, vol. 4, no. 5, pp. 612–620, 2023, https://doi.org/10.18196/jrc.v4i5.19448.

[21] R. P. Borase, D. K. Maghade, S. Y. Sondkar, and S. N. Pawar, "A review of PID control, tuning methods and applications," *International Journal of Dynamics and Control*, vol. 9, no. 2, pp. 818-827, 2021, https://doi.org/10.1007/s40435-020-00665-4.

[22] R. R. Alla, N. Lekyasri, and K. Rajani, "PID Control Design for Second Order Systems," *International Journal of Engineering and Manufacturing (IJEM)*, vol. 9, no. 4, pp. 45-56, 2019, https://doi.org/10.5815/ijem.2019.04.04.

[23] E. W. Suseno and A. Ma'arif, "Tuning of PID controller parameters with genetic algorithm method on DC motor," *International Journal of Robotics and Control Systems (IJRCS),* vol. 1, no. 1, pp. 41-53, 2021, https://doi.org/10.31763/ijrcs.v1i1.249.

[24] E. S. Ghith and F. A. A. Tolba, "Design and optimization of PID controller using various algorithms for micro-robotics system," *Journal of Robotics and Control (JRC)*, vol. 3, no. 3, pp. 244-256, 2022, https://doi.org/10.18196/jrc.v3i3.14827.

[25] S. J. Hammoodi, K. S. Flayyih, and A. R. Hamad, "Design and Implementation of Speed Control System for DC Motor Based on PID Control and Matlab Simulink," *International Journal of Power Electronics and Drive Systems*, vol. 11, no. 1, pp. 127-134, 2020, https://doi.org/10.11591/ijpeds.v11.i1.

[26] D. S. Febriyan and R. D. Puriyanto, "Implementation of DC motor PID control on conveyor for separating potato seeds by weight," *International Journal of Robotics and Control Systems (IJRCS)*, vol. 1, no. 1, pp. 15-26, 2021, https://doi.org/10.31763/ijrcs.v1i1.221.

[27] E. S. Rahayu, A. Ma'arif, and A. Çakan, "Particle swarm optimization (PSO) tuning of PID control on DC motor," *International Journal of Robotics and Control Systems (IJRCS)*, vol. 2, no. 2, pp. 435-447, 2022, https://doi.org/10.31763/ijrcs.v2i2.476.

[28] Z. Qi, Q. Shi, and H. Zhang, "Tuning of Digital PID Controllers Using Particle Swarm Optimization Algorithm for a CAN-Based DC Motor Subject to Stochastic Delays," *IEEE Transactions on Industrial Electronics*, vol. 67, no. 7, pp. 5637-5646, 2019, https://doi.org/10.1109/TIE.2019.2934030.

[29] M. Jain, V. Saihjpal, N. Singh, and S. B. Singh, "An overview of variants and advancements of PSO algorithm," *Applied Sciences*, vol. 12, no. 17, Art. no. 8392, 2022, https://doi.org/10.3390/app12178392.

[30] D. D. Ramírez-Ochoa, L. A. Pérez-Domínguez, E. A. Martínez-Gómez, and D. Luviano-Cruz, "PSO, a swarm intelligence-based evolutionary algorithm as a decision-making strategy: A review," *Symmetry*, vol. 14, no. 3, Art. no. 455, 2022, https://doi.org/10.3390/sym14030455.

[31] S. Mahfoud, A. Derouich, N. El Ouanjli, M. El Mahfoud, and M. Taoussi, "A New Strategy-Based PID Controller Optimized by Genetic Algorithm for DTC of the Doubly Fed Induction Motor," *Systems*, vol. 9, no. 2, p. 37, 2021, https://doi.org/10.3390/systems9020037.

[32] B. Song, R. Wang, and L. Xu, "Design of PMSM Dual-Loop Control Systems Integrating LADRC and PI Controllers via an Improved PSO Algorithm," *International Transactions on Electrical Energy Systems*, 2024, https://doi.org/10.1155/2024/9378284.

[33] M. M. Nishat, F. Faisal, A. J. Evan, M. M. Rahaman, M. S. Sifat, and H. F. Rabbi, "Development of genetic algorithm (GA) based optimized PID controller for stability analysis of DC-DC buck converter," *Journal of Power and Energy Engineering*, vol. 8, no. 9, pp. 1–8, 2020, https://doi.org/10.4236/jpee.2020.89002.

[34] M. G. Abdolrasol, A. Ayob, A. H. Mutlag, and T. S. Ustun, "Optimal fuzzy logic controller based PSO for photovoltaic system," *Energy Reports*, vol. 9, pp. 427-434, 2023, https://doi.org/10.1016/j.egyr.2022.11.039.

[35] K. Vanchinathan and N. Selvaganesan, "Adaptive Fractional Order PID Controller Tuning for Brushless DC Motor Using Artificial Bee Colony Algorithm," *Control and Optimization*, vol. 4, 2021, https://doi.org/10.1016/j.rico.2021.100032.

[36] P. Mohindru, "Review on PID, fuzzy and hybrid fuzzy PID controllers for controlling non-linear dynamic behaviour of chemical plants," *Artificial Intelligence Review*, vol. 57, Art. no. 97, 2024, https://doi.org/10.1007/s10462-024-10743-0.

[37] S. Gobinath and M. Madheswaran, "Deep Perceptron Neural Network with Fuzzy PID Controller for Speed Control and Stability Analysis of BLDC Motor," *Soft Computing*, vol. 24, no. 13, pp. 10161-10180, 2020, https://doi.org/10.1007/s00500-019-04532-z.

[38] J. S. Wang and C. G. Lee, "Self-adaptive neuro-fuzzy inference systems for classification applications," *IEEE Transactions on Fuzzy systems*, vol. 10, no. 6, pp. 790-802, 2002, https://doi.org/10.1109/TFUZZ.2002.805880.

[39] M. K. Saleem, M. L. U. R. Shahid, A. Nouman, H. Zaki, and M. A. U. R. Tariq, "Design and implementation of adaptive neuro-fuzzy inference system for the control of an uncertain ball and beam

apparatus," *Mehran University Research Journal of Engineering & Technology*, vol. 41, no. 2, pp. 178–184, 2022, https://doi.org/10.22581/muet1982.2202.17.

[40] M. Kiew-ong-art, P. Chotikunnan, A. Wongkamhang, R. Chotikunnan, A. Nirapai, P. Imura, M. Sangworasil, N. Thongpance, and A. Srisiriwat, "Comparative Study of Takagi-Sugeno-Kang and Madani Algorithms in Type-1 and Interval Type-2 Fuzzy Control for Self-Balancing Wheelchairs," *International Journal of Robotics and Control Systems (IJRCS)*, vol. 3, no. 4, pp. 643-657, 2023, https://doi.org/10.31763/ijrcs.v3i4.1154.

[41] P. Chotikunnan, R. Chotikunnan, A. Nirapai, A. Wongkamhang, P. Imura, and M. Sangworasil, "Optimizing Membership Function Tuning for Fuzzy Control of Robotic Manipulators Using PID-Driven Data Techniques," *Journal of Robotics and Control (JRC)*, vol. 4, no. 2, pp. 128-140, 2023, https://doi.org/10.18196/jrc.v4i2.18108.

[42] A. M. Lopes and L. Chen, "Fractional order systems and their applications," *Fractal and Fractional*, vol. 6, no. 7, Art. no. 389, 2022, https://doi.org/10.3390/fractalfract6070389.

[43] D. Li and J. Dong, "Fractional-order systems optimal control via actor-critic reinforcement learning and its validation for chaotic MFET," *IEEE Transactions on Automation Science and Engineering*, 2024, https://doi.org/10.1109/TASE.2024.3361213.

[44] K. Sayed, H. H. El-Zohri, A. Ahmed, and M. Khamies, "Application of Tilt Integral Derivative for Efficient Speed Control and Operation of BLDC Motor Drive for Electric Vehicles," *Fractal and Fractional*, vol. 8, no. 1, p. 61, 2024, https://doi.org/10.3390/fractalfract8010061.

[45] V. Kumarasamy, V. KarumanchettyThottam Ramasamy, G. Chandrasekaran, et al., "A review of integer order PID and fractional order PID controllers using optimization techniques for speed control of brushless DC motor drive," *International Journal of System Assurance Engineering and Management*, vol. 14, pp. 1139-1150, 2023, https://doi.org/10.1007/s13198-023-01952-x.

[46] Z. U. A. Zafar, N. Ali, and C. Tunç, "Mathematical modeling and analysis of fractional-order brushless DC motor," *Advances in Difference Equations*, vol. 2021, no. 433, 2021, https://doi.org/10.1186/s13662-021-03587-3.

[47] P. Dutta and S. K. Nayak, "Grey Wolf Optimizer Based PID Controller for Speed Control of BLDC Motor," *Journal of Electrical Engineering & Technology*, vol. 16, no. 2, pp. 955-961, 2021, https://doi.org/10.1007/s42835-021-00660-5.

[48] S. Wang, X. Zhao, and Q. Yu, "Vehicle stability control strategy based on recognition of driver turning intention for dual-motor drive electric vehicle," *Mathematical Problems in Engineering*, vol. 2020, Art. no. 3143620, https://doi.org/10.1155/2020/3143620.

[49] T. Triwiyanto, W. Caesarendra, V. Abdullayev, A. A. Ahmed, and H. Herianto, "Single lead EMG signal to control an upper limb exoskeleton using embedded machine learning on Raspberry Pi," *Journal of Robotics and Control (JRC)*, vol. 4, no. 1, pp. 35-45, 2023, https://doi.org/10.18196/jrc.v4i1.17364.

[50] H. Torres-Salinas, J. Rodríguez-Reséndiz, E. E. Cruz-Miguel, and L. A. Ángeles-Hurtado, "Fuzzy logic and genetic-based algorithm for a servo control system," *Micromachines*, vol. 13, no. 4, Art. no. 586, 2022, https://doi.org/10.3390/mi13040586.

[51] M. Luo, J. A. Duan, and Z. Yi, "Speed tracking performance for a coreless linear motor servo system based on a fitted adaptive fuzzy controller," *Energies*, vol. 16, no. 3, Art. no. 1259, 2023, https://doi.org/10.3390/en16031259.

[52] S. W. Shneen, H. S. Dakheel, and Z. B. Abdullah, "Design and implementation of no load, constant and variable load for DC servo motor," *Journal of Robotics and Control (JRC)*, vol. 4, no. 3, pp. 323-329, 2023, https://doi.org/10.18196/jrc.v4i3.17387.

[53] M. A. Abdelghany, A. O. Elnady, and S. O. Ibrahim, "Optimum PID controller with fuzzy self-tuning for DC servo motor," *Journal of Robotics and Control (JRC)*, vol. 4, no. 4, pp. 500-508, 2023, https://doi.org/10.18196/jrc.v4i4.18676.

[54] F. N. Abdullah, G. A. Aziz, and S. W. Shneen, "Simulation model of servo motor by using MATLAB," *Journal of Robotics and Control (JRC)*, vol. 3, no. 2, pp. 176-179, 2022, https://doi.org/10.18196/jrc.v3i2.13959.

[55] M. R. Islam, M. R. T. Hossain, and S. C. Banik, "Synchronizing of stabilizing platform mounted on a two-wheeled robot," *Journal of Robotics and Control (JRC)*, vol. 2, no. 6, pp. 552-558, 2021, https://doi.org/10.18196/jrc.26136.

[56] A. O. Amole, O. E. Olabode, D. O. Akinyele, and S. G. Akinjobi, "Optimal temperature control scheme for milk pasteurization process using different tuning techniques for a proportional integral derivative controller," *Iranian Journal of Electrical & Electronic Engineering*, vol. 18, no. 3, pp. 1–16, 2022, https://doi.org/10.22068/IJEEE.18.3.2170.

[57] P. Saini and C. Sharma, "Comparative Analysis of Controller Tuning Techniques for Dead Time Processes," *International Journal of Mathematical, Engineering and Management Sciences*, vol. 4, no. 3, pp. 803-813, 2019, https://doi.org/10.33889/IJMEMS.2019.4.3-063.

[58] A. W. Hidayat, I. Sulistiyowati, A. Wicaksono, and S. Syahrorini, "Hybrid system prototype for dam water level control system to irrigating rice fields," *Buletin Ilmiah Sarjana Teknik Elektro*, vol. 6, no. 1, pp. 25-33, 2024, https://doi.org/10.12928/biste.v6i1.10016.

[59] E. H. Kadhim and A. T. Abdulsadda, "Mini drone linear and nonlinear controller system design and analyzing," *Journal of Robotics and Control (JRC)*, vol. 3, no. 2, pp. 212-218, 2022, https://doi.org/10.18196/jrc.v3i2.14180.

[60] A. K. Hado, B. S. Bashar, M. M. A. Zahra, R. Alayi, Y. Ebazadeh, and I. Suwarno, "Investigating and optimizing the operation of microgrids with intelligent algorithms," *Journal of Robotics and Control (JRC)*, vol. 3, no. 3, pp. 279-288, 2022, https://doi.org/10.18196/jrc.v3i3.14772.

[61] D. Kumar, R. Malhotra, and S. R. Sharma, "Design and construction of a smart wheelchair," *Procedia Computer Science*, vol. 172, pp. 302-307, 2020, https://doi.org/10.1016/j.procs.2020.05.048.

[62] F. Ahmmed, A. Rahman, A. Islam, A. Alaly, S. Mehnaj, P. Saha, and T. Hossain, "Arduino-controlled multi-function robot with Bluetooth and nRF24L01+ communication," *International Journal of Robotics and Control Systems (IJRCS)*, vol. 4, no. 3, pp. 1353-1381, 2024, https://doi.org/10.31763/ijrcs.v4i3.1517.

[63] A. Prasetyo, J. Jamaaluddin, and I. Anshory, "PCB (Printed Circuit Board) etching machine using ESP32-camera based Internet of Things," *Buletin Ilmiah Sarjana Teknik Elektro*, vol. 5, no. 2, pp. 260–268, 2023, https://doi.org/10.32492/jeetech.v4i2.4208.

[64] Y. Irawan, M. Muhardi, R. Ordila, and R. Diandra, "Automatic floor cleaning robot using Arduino and ultrasonic sensor," *Journal of Robotics and Control (JRC)*, vol. 2, no. 4, pp. 240-243, 2021, https://doi.org/10.18196/jrc.2485.

[65] Y. Irawan, R. Wahyuni, and H. Fonda, "Folding clothes tool using Arduino Uno microcontroller and gear servo," *Journal of Robotics and Control (JRC)*, vol. 2, no. 3, pp. 170-174, 2021, https://doi.org/10.18196/jrc.2373.

[66] M. H. Zulwidad and I. Sulistiyowati, "Efficiency through automation: A single system for multiple railway guard posts," *Buletin Ilmiah Sarjana Teknik Elektro*, vol. 5, no. 3, pp. 407-416, 2023, https://doi.org/10.12928/biste.v5i3.9001.

[67] M. Meindl, R. Mönkemöller, and T. Seel, "Autonomous iterative motion learning (AI-MOLE) of a SCARA robot for automated myocardial injection," *IFAC-PapersOnLine*, vol. 58, no. 24, pp. 380–385, 2024, https://doi.org/10.1016/j.ifacol.2024.11.067.

[68] Y. Lv, X. Ren, J. Tian, and X. Zhao, "Inverse-model-based iterative learning control for unknown MIMO nonlinear system with neural network," *Neurocomputing*, vol. 519, pp. 187–193, 2023, https://doi.org/10.1016/j.neucom.2022.11.040.

[69] G. Wu, B. Niu, and Q. Li, "Trajectory tracking control of fast parallel SCARA robots with fuzzy adaptive iterative learning control for repetitive pick-and-place operations," *Electronics*, vol. 12, no. 24, p. 4995, 2023, https://doi.org/10.3390/electronics12244995.

[70] B. Panomruttanarug, R. W. Longman, and M. Q. Phan, "Steady state frequency response design of finite time iterative learning control," *The Journal of the Astronautical Sciences*, vol. 67, no. 2, pp. 571–594, 2020, https://doi.org/10.1007/s40295-019-00198-9.

[71] B. Panomruttanarug, "Position control of robotic manipulator using repetitive control based on inverse frequency response design," *International Journal of Control, Automation and Systems*, vol. 18, no. 11, pp. 2830–2841, 2020, https://doi.org/10.1007/s12555-019-0518-2.

[72] P. Chotikunnan, B. Panomruttanarug, and P. Manoonpong, "Dual design iterative learning controller for robotic manipulator application," *Journal of Control Engineering and Applied Informatics*, vol. 24, no. 3, pp. 76–85, 2022, https://ceai.srait.ro/index.php?journal=ceai&page=article&op=view&path%5B%5D=7786.

[73] R. Chotikunnan, P. Chotikunnan, Y. Pititheeraphab, and P. Minyong, "Time-varying sign gain with expert system in serial iterative learning control architecture," *International Review of Automatic Control*, vol. 17, no. 1, pp. 1–9, 2024, https://doi.org/10.15866/ireaco.v17i1.24739.

[74] P. Chotikunnan, K. Roongprasert, R. Chotikunnan, Y. Pititheeraphab, T. Puttasakul, A. Wongkamhang, and N. Thongpance, "Hybrid fuzzy-expert system control for robotic manipulator applications," *Journal of Robotics and Control (JRC)*, vol. 6, no. 1, pp. 155–165, 2025, https://doi.org/10.18196/jrc.v6i1.24956.

[75] F. Umam, A. Dafid, and A. D. Cahyani, "Implementation of Fuzzy Logic Control Method on Chilli Cultivation Technology Based Smart Drip Irrigation System," *Jurnal Ilmiah Teknik Elektro Komputer dan Informatika*, vol. 9, no. 1, pp. 132-141, 2023, https://doi.org/10.26555/jiteki.v9i1.25813.

[76] O. T. Altinoz and A. E. Yilmaz, "Investigation of the Optimal PID-Like Fuzzy Logic Controller for Ball and Beam System with Improved Quantum Particle Swarm Optimization," *International Journal of Computational Intelligence and Applications*, vol. 21, no. 4, p. 2250025, 2022, https://doi.org/10.1142/s1469026822500250.

[77] V. Velmurugan, M. Venkatesan, and N. Praboo, "Analysis and performance validation of CRONE controllers for speed control of a DC motor," *International Journal of Robotics and Control Systems (IJRCS)*, vol. 4, no. 2, pp. 558-580, 2024, https://doi.org/10.31763/ijrcs.v4i2.1343.

[78] N. Ramadhani, A. Ma'arif, and A. Çakan, "Implementation of PID control for angular position control of Dynamixel servo motor," *Control Systems and Optimization Letters*, vol. 2, no. 1, pp. 8-14, 2024, https://doi.org/10.59247/csol.v2i1.40.

[79] A. Muqaffi Siswanto and M. Muchlas, "Prototype of automatic sorting of goods in cosmetics warehouse," *Buletin Ilmiah Sarjana Teknik Elektro*, vol. 4, no. 3, pp. 142-151, 2023, https://doi.org/10.12928/biste.v4i3.6919.

[80] K. Kunal, A. Z. Arfianto, J. E. Poetro, F. Waseel, and R. A. Atmoko, "Accelerometer implementation as feedback on 5 degree of freedom arm robot," *Journal of Robotics and Control (JRC)*, vol. 1, no. 1, pp. 31-34, 2020, https://doi.org/10.18196/jrc.1107.

[81] K. Khairunisa, M. Mardeni, and Y. Irawan, "Smart aquarium design using Raspberry Pi and Android based," *Journal of Robotics and Control (JRC)*, vol. 2, no. 5, pp. 368-372, 2021, https://doi.org/10.18196/jrc.25109.